



## Full Text View

[Volume 30, Issue 9 \(September 2000\)](#)

### Journal of Physical Oceanography

Article: pp. 2320–2341 | [Abstract](#) | [PDF \(1.53M\)](#)

# Estimates of Area-Averaged Diapycnal Fluxes from Basin-Scale Budgets

**Bernadette M. Sloyan**

*Antarctic Cooperative Research Centre, and Institute of Antarctic and Southern Ocean Studies, University of Tasmania, Hobart, Tasmania, Australia*

**Stephen R. Rintoul**

*Antarctic Cooperative Research Centre, University of Tasmania, and CSIRO Division of Marine Research, Hobart, Tasmania, Australia*

(Manuscript received October 22, 1998, in final form November 4, 1999)

DOI: 10.1175/1520-0485(2000)030<2320:EOAADF>2.0.CO;2

### ABSTRACT

Estimates of area-averaged diapycnal fluxes for the southern oceans are derived from basin-scale budgets of mass, heat, and salt using a box inverse model. The diapycnal fluxes are found to be significant terms in the isopycnal budgets of mass, heat, and salt. Dense water entering the subtropical Indian and Pacific basins from the south is returned below the thermocline as less dense deep water. In the Southern Ocean deep water is converted to denser deep and bottom water. Water properties at intermediate depth are substantially modified by diapycnal fluxes of heat and salt, but the modification of intermediate water is not solely driven by interior mixing. The inferred fluxes help explain the changes in temperature–salinity curves observed across each basin, and they are consistent with our understanding of the overall three-dimensional circulation of the Southern Ocean.

The fact that area-averaged diapycnal fluxes can be determined from basin-scale budgets using a suitably designed inverse model is encouraging: similar methods applied to the high-quality measurements collected during the World Ocean Circulation Experiment promise to provide the first global maps of diapycnal fluxes derived from ocean observations.

### 1. Introduction

Diapycnal fluxes of mass, heat, salt, and other properties are a key element of the global ocean circulation. For example, the global overturning circulation associated

#### Table of Contents:

- [Introduction](#)
- [The box inverse method](#)
- [Representing diapycnal](#)
- [Diapycnal fluxes in the](#)
- [Discussion](#)
- [Conclusions](#)
- [REFERENCES](#)
- [APPENDIX](#)
- [TABLES](#)
- [FIGURES](#)

#### Options:

- [Create Reference](#)
- [Email this Article](#)
- [Add to MyArchive](#)
- [Search AMS Glossary](#)

#### Search CrossRef for:

- [Articles Citing This Article](#)

#### Search Google Scholar for:

- [Bernadette M. Sloyan](#)
- [Stephen R. Rintoul](#)

with the sinking and export of North Atlantic Deep Water (NADW) must be closed by upwelling across isopycnals somewhere else in the ocean. However, the upwelling rate is too small to observe directly. Given the lack of observational evidence of where the required upwelling occurred, [Stommel and Arons \(1960\)](#) developed a theory of the deep ocean circulation based on the assumption of uniform upwelling throughout the World Ocean. [Gordon \(1986\)](#) showed that the assumption of uniform upwelling implied a central role for interbasin exchange provided by the Indonesian Throughflow and Agulhas retroflection in the global NADW cell.

More recently, direct observations of microstructure in the ocean interior suggest that diapycnal mixing, and hence upwelling, is generally weak and spatially nonuniform ([Polzin et al. 1997](#)). Nonuniform upwelling suggests a very different deep circulation than proposed by [Stommel and Arons \(1960\)](#). The very weak diapycnal mixing observed in the interior away from rough topography has renewed interest in the possibility that mixing near the boundaries of the ocean dominates the net diapycnal mixing ([Wunsch 1970](#); [Armi 1978](#)). Another possibility is that much of the diapycnal transformation required to close the NADW cell occurs through air–sea forcing where isopycnals outcrop at high latitudes in the Southern Ocean ([Döös and Coward 1997](#); [Toggweiler and Samuels 1998](#)). Our ideas about the general circulation of the ocean will remain incomplete until we have a better understanding of where the essential diapycnal fluxes occur.

It is generally accepted that it is not feasible to directly observe diapycnal fluxes, except perhaps in local areas using special instrumentation. The purpose of this paper is to demonstrate that a suitably constructed box inverse model can determine area-averaged diapycnal fluxes with some skill. That this is so should perhaps not come as a surprise: the net diapycnal fluxes occurring over large areas of the ocean are balanced by lateral (isopycnal) fluxes of properties—a model cannot estimate the latter well (e.g., determine the meridional heat flux across a hydrographic section) without capturing the diapycnal fluxes as well.

A number of prior inverse studies have estimated diapycnal fluxes, using a variety of parameterizations ([Wunsch et al. 1983](#); [Wunsch 1984](#); [Hogg 1987](#); [Schlitzer 1987](#); [Roemmich and McCallister 1989](#)). In this study we follow the suggestions of [McIntosh and Rintoul \(1997\)](#) and parameterize the diapycnal fluxes by an independent diapycnal flux unknown for each property. We apply this parameterization of the diapycnal property fluxes to an inversion of the Southern Ocean. The net fluxes across isopycnals on basin scales are found to be significant terms in the overall budgets for isopycnal layers.

## 2. The box inverse method

The box inverse method introduced by [Wunsch \(1978\)](#) uses two oceanographic techniques to define the general circulation: simple dynamics and water mass analysis. The ocean is assumed to be in hydrostatic, geostrophic, and hence thermal wind, balance. Integrating the thermal wind equation from a depth  $z_0$  gives the velocity between two adjacent stations along a hydrographic section:

$$v(x, z) = \frac{-g}{\rho_0 f} \int_{z_0}^z \frac{\partial \rho}{\partial x} dz + v(x, z_0) = v_r + b. \quad (1)$$

The baroclinic or relative velocity ( $\mathbf{v}_r$ ) is determined from the hydrographic data but the barotropic or reference velocity ( $b$ ) is unknown.

In order to solve for  $b$ , [Wunsch \(1978\)](#) defined a closed volume of ocean, or “box” bounded by hydrographic sections and land barriers. Within the region he assumed that mass was conserved in discrete horizontal layers enabling a set of conservation equations to be written. Further development of inverse techniques has resulted in the inclusion of heat, salt, and nutrients to the suite of conserved properties and the inclusion of additional unknowns, such as diapycnal fluxes and diffusivities ([Wunsch et al. 1983](#); [Fu 1986](#); [Rintoul and Wunsch 1990](#); [Macdonald 1991](#); [Rintoul 1991](#)).

The resulting system of conservation equations can be written in matrix form as

$$\mathbf{A}\mathbf{b} = \mathbf{d}. \quad (2)$$

Here  $\mathbf{A}$  is a matrix whose elements are the area  $\times$  property concentration ( $C$ ) at each station pair in each layer, and for each layer interface;  $\mathbf{d}$  is the property divergence in each layer due to relative ( $\Delta x_j \times C_j \mathbf{v}_r$ ) and Ekman ( $E_j C_j$ ) fluxes; and  $\mathbf{b}$  is the vector of unknown reference velocities ( $b_j$ ) and diapycnal “velocities” ( $w_m^*$ ). In the oceanographic context the linear system generally has more unknowns than equations—an underdetermined problem that has an infinite number of solutions. A least squares technique is generally used to find a particular solution.

The data used in inverse methods contain errors (e.g., from nonsynoptic data, measurement error, and aliasing), which

results in  $\mathbf{A}\mathbf{A}^T$  being singular. To solve such a system of equations the singular value decomposition (SVD) is used (Lanczos 1961). The SVD decomposes  $\mathbf{A}$  into a coupled eigenvector–eigenvalue problem (Wunsch 1978). The particular solution chosen is the one where the deviation from the initial choice of  $\mathbf{b}$  is small (solution norm  $\|\mathbf{b}\|$ ) given the misfit of each equation (residual norm  $\|\mathbf{A}\mathbf{b} - \mathbf{d}\|$ ) is reduced to a reasonable value. For a more thorough description of inverse methods the reader is referred to Wunsch (1978, 1996).

Since the solution minimizes the departure from an initial guess, it is important to use whatever knowledge exists to make the best initial guess possible. Water mass analysis is an important tool for defining the initial choice of reference level. For example, the reference level (usually a “level of no motion” where  $b = 0$ ) is generally assumed to coincide with the boundary between water masses that flow in opposing directions, for example, the boundary between North Atlantic Deep Water and Antarctic Bottom Water in the Atlantic. Other prior information (e.g., an estimate of the transport of a strong boundary current) provides additional important information that can be included in the initial guess.

### 3. Representing diapycnal fluxes in box inverse models

Diapycnal fluxes have been represented in previous box inverse studies in various ways. Early inversions ignored diapycnal fluxes (e.g., Wunsch 1978). The layer residuals in inversions that do not explicitly include diapycnal fluxes in the conservation equations have sometimes been integrated vertically to determine the implied diapycnal fluxes (e.g., Wunsch et al. 1983; Roemmich and McCallister (1989)). Most commonly, the diapycnal fluxes have been represented by a single unknown for each interface, which is interpreted as the net flux resulting from all processes that can carry properties across isopycnals, including advection, diffusion, cabelling, and other eddy process (e.g., Wunsch 1984). The same unknown usually appears in each property equation, multiplied by the layer interface area and the mean tracer concentration on the interface (i.e., if  $w_m^*$  is the net diapycnal mass flux across a layer, the heat flux is given by  $w_m^* \bar{\theta}$ , where  $\bar{\theta}$  is the mean potential temperature on the interface). Finally, some inversions have separated the net diapycnal flux into advective and diffusive contributions, where the diapycnal diffusivity becomes an additional unknown (which is often required to be positive, consistent with downgradient Fickian diffusion) (Hogg 1987; Schlitzer 1987; Tziperman and Hecht 1988).

Given that direct observations of the net diapycnal flux across large areas of ocean are not possible, it is difficult to assess the skill with which models such as those cited above determine diapycnal fluxes. McIntosh and Rintoul (1997) used output from the FRAM (Fine Resolution Antarctic Model) model to test how well a box inverse model can determine diapycnal (and lateral) fluxes. The lessons of their study can be summarized as follows. 1) In FRAM the diapycnal fluxes are a large term in the property budgets; ignoring them leads to large errors in lateral transport estimates, as the reference level velocity is adjusted to remove imbalances, which are in reality due to divergence of diapycnal fluxes. 2) Diapycnal fluxes cannot be reliably estimated by integrating vertically the layer residuals in box models, which do not explicitly include diapycnal fluxes. The SVD solution tends to leave residuals of equal magnitude in each layer; in FRAM, the divergence of the lateral fluxes into each layer are not of equal magnitude so that the residuals in models that neglect diapycnal fluxes are not a good representation of the diapycnal fluxes. More physically, the diapycnal fluxes are linked between boxes—flow out of one layer is flow into an adjacent layer—while the residuals are not. 3) Explicitly including the diapycnal fluxes improved the conditioning of the problem, and hence decreased the sensitivity of the solution to error. 4) Fluxes due to the correlation between spatial variations of diapycnal velocity and of tracer concentration on an isopycnal surface are significant in FRAM, may differ in sign from the explicit diffusion (caused in the model by both vertical and horizontal diffusion across sloping isopycnals), and are not related to the vertical tracer gradients. As a result, the diapycnal flux carried by processes other than mean advection across the isopycnal is not well represented as Fickian diffusion, nor is the net diapycnal flux well represented by the mean advection across the surface multiplied by the mean tracer concentration on the surface.

Based on these findings, McIntosh and Rintoul (1997) chose to represent the net diapycnal flux across each interface as a separate unknown for each property [ $w_c^* = (w_m^*, w_t^*, w_s^*)$ ]. McIntosh and Rintoul (1997) did not explore the spatial distribution of the diapycnal fluxes in FRAM, experiment with alternate representations of the diapycnal fluxes in the box inverse model, or apply the box inverse to real ocean observations.

Before determining the most appropriate parameterization of the diapycnal fluxes in the Southern Ocean inverse model, we considered some of the issues not addressed by McIntosh and Rintoul (1997) (see appendix). This study was particularly concerned with alternative representations of the diapycnal fluxes and their spatial distribution. In our FRAM experiments we find that solving either for the net diapycnal flux (as McIntosh and Rintoul 1997) or for the diapycnal velocity and implied property diffusivities can accurately reproduce the “true” fluxes. Using the latter approach we have seen that the “effective diffusivity” is not the same for heat and salt and that the diffusivities vary in space. The spatial variations in diffusivity are particularly influenced by “eddy” ( $e'c'$ ) fluxes, where  $e'c'$  represents the flux carried by spatial correlations between the deviations of velocity and tracer concentration from their mean value on the isopycnal. The  $e'c'$  fluxes are largest in regions where the layers outcrop or undercrop and in regions of high eddy variability. Particular care should be taken when interpreting the “effective diffusivity” in such regions: the inferred diffusivity may be different for different properties, may

be negative, and will vary in space. In other words, parameterization of effective diffusion by Fick's law may not be appropriate if the "eddy" ( $e'c'$ ) contribution is significant. This study suggests that a straightforward and consistent method to parameterize the diverse mix of processes responsible for the net diapycnal fluxes across the large interface areas typical of most box models is to solve for the net flux by including an independent diapycnal flux unknown for each property.

FRAM, or any other numerical model, of course does not provide us with a perfect representation of the real ocean. Therefore, although numerical models can provide guidance concerning how best to parameterize the diapycnal fluxes, the ultimate test of the parameterization is to apply it in an inverse model with real hydrographic data, and check whether the derived diapycnal and lateral fluxes are consistent with observations and prior oceanographic understanding.

#### 4. Diapycnal fluxes in the Southern Ocean

In this section we show results of using the inverse model described above to determine the circulation and water mass transformation in the Southern Ocean. While the focus here is on the diapycnal fluxes, first a brief overview of the circulation is given to familiarize the reader with the gross features of the model, and to demonstrate that the lateral fluxes are generally consistent with earlier estimates. A complete description of the design and results of the inverse model can be found in [Sloyan \(1997\)](#), [Sloyan and Rintoul \(2000\)](#), and [Sloyan and Rintoul \(2000, manuscript submitted to \*J. Phys. Oceanogr.\*\)](#).

##### *a. The model: A priori constraints and errors*

The conservation equations take the basic form described in the preceding sections. [Table 1](#) gives the name, year, and season of the sections used in this study while [Fig. 1](#) shows the location of the hydrographic sections and the "boxes" they define. The sections in this study are recent high quality hydrographic sections, apart from the Ind18 section. The sections across the Pacific, in Drake Passage and south of Australia are part of the World Ocean Circulation Experiment dataset.

Twenty-three layers, bounded by 22 neutral surfaces, are used in the Southern Ocean inversion. The layers are defined by neutral density surfaces calculated using the [Jackett and McDougall \(1997\)](#) algorithm. Across the zonal sections (SAVE2, SAVE4, Ind18, Ind32, and Pac32) the initial reference level is the boundary between the northward flowing Antarctic Bottom Water– Lower Circumpolar Deep Water (AABW/LCDW) and southward flowing North Atlantic Deep Water, Indian Deep Water (IDW), or Pacific Deep Water (PDW), although in the Argentine basin of SAVE4 the reference level is taken as the deepest common depth. At the three Southern Ocean choke point sections (DrakeP, SAfrica, and SAust) a deepest common reference level is chosen.

A novel addition to the inverse model is the explicit inclusion of air–sea fluxes of heat and freshwater, and the water mass transformations they drive. The technique follows the strategy of [Walín \(1982\)](#) and [Speer and Tziperman \(1992\)](#). The air–sea fluxes result in a net buoyancy flux, which can be integrated over the area of an outcropping isopycnal layer to compute the net water mass transformation, that is, the transfer between layers. Corrections to the air–sea fluxes are included as additional unknowns in the inversion. The climatological data used to calculate the air–sea property convergences are: Comprehensive Ocean–Atmosphere Data Set heat flux ([da Silva et al. 1994](#)), wind stress ([Hellerman and Rosenstein 1983](#)), and freshwater from the Global Assimilation and Prediction System ([Budd et al. 1995](#)). We use [Levitus and Boyer \(1994\)](#) to find the outcropping position of the neutral density surfaces for each month, the weighted mean temperature and salinity of the Ekman layer, and the annual mean depth and property concentration on the neutral surfaces in the interior of each box. A complete description of the method and estimates of the water mass transformation driven by the air–sea fluxes can be found in [Sloyan \(1997\)](#) and [Sloyan and Rintoul \(2000\)](#). Here we focus on the diapycnal fluxes due to processes in the "interior" of the ocean, where interior means everything below the surface skin; the interior diapycnal fluxes include horizontal fluxes across the nearly vertical isopycnals in the mixed layer, for example, but exclude the fluxes driven by air–sea forcing.

[Table 2](#) contains information on the a priori constraints applied to the inverse model. [Peterson and Whitworth \(1989\)](#) and [Peterson \(1992\)](#) find large bottom velocities beneath the Malvinas Current, which increase the transport substantially above that estimated from geostrophy relative to a deep reference level. This information is included by setting the initial guess of the reference velocity at the first six station pairs adjacent to the South American coast to  $0.132 \text{ m s}^{-1}$  ( $13.2 \text{ cm s}^{-1}$ ), comparable to observations from near-bottom current meters in this region ([Peterson and Whitworth 1989](#); [Peterson 1992](#)). Mooring array PCM-9 was deployed in a 1000-km line east of the Tonga–Kermadec Ridge. The PCM-9 transport constraint is applied to deep and bottom layers (18 to 23) at stations that span the longitude range on the mooring array ( $167.5^\circ$ – $179^\circ\text{W}$ ). Total box silica conservation is a weak constraint, reflecting the uncertainty in the silica flux. The importance of appropriate column and row weighting has been discussed by [McIntosh and Rintoul \(1997\)](#).

To explore whether the constraints on individual layers provide significant information, an experiment was run that

conserves only total mass and satisfies additional a priori constraints (Table 2) and a southward net transport of  $10 \times 10^6 \text{ m}^3 \text{ s}^{-1}$  across Ind18. The results show that although the net lateral and zonal mass fluxes agree with previous estimates of these quantities, there are some unrealistic features of the circulation of individual water mass layers. Closer examination of the implied water mass circulation shows that at SAVE2 and SAVE4 the southward flux of  $15.9 \pm 5.5 \times 10^6 \text{ m}^3 \text{ s}^{-1}$  of NADW (layer 16 to 18) principally occurs in the eastern basins of the Atlantic Ocean and not at the western boundary. At  $32^\circ\text{S}$  in the Indian Ocean there is a southward transport of deep and bottom waters in the Mozambique Basin that is associated with low temperature, higher oxygen concentration Antarctic waters. In the eastern regions, over the Ninetyeast ridge, Broken Plateau, and in the Perth Basin there is a northward transport throughout the entire water column even in the low oxygen concentration water masses of Indian Deep Water. At  $32^\circ\text{S}$  in the Pacific there is a net southward transport of higher oxygen Lower Circumpolar Deep Water (layer 18). The southward transport of  $30.1 \pm 4.7 \times 10^6 \text{ m}^3 \text{ s}^{-1}$  of Pacific Deep Water and LCDW (layer 18) is balanced by northward transport of thermocline and Antarctic Intermediate Waters and Antarctic deep and bottom water (layers 19–23), implying a large conversion of thermocline and intermediate water to deep water in the northern Pacific Ocean. In the Southern Ocean south of Australia there is no westward flow of extreme Antarctic Lower Bottom Water (ALBW), while a large convergence ( $8 \times 10^6 \text{ m}^3 \text{ s}^{-1}$ ) of AABW between southern Africa and Australia suggests that the Southern Ocean Indian sector produces an equivalent volume of AABW as the Weddell Sea.

The rows are weighted by the property norm and the columns are weighted by the area norm. A scaling factor is also applied to the reference velocity unknowns, the diapycnal property flux unknowns, and air–sea climatology corrections such that the condition number (the ratio of largest eigenvalue to smallest eigenvalue) is minimized. Errors due to the combination of nonsynoptic hydrographic sections and Levitus data in this model result in choosing a rank where the equation residual norms are of  $O[1 \text{ to } 2 (\times 10^6 \text{ m}^3 \text{ s}^{-1})]$ .

The errors given in the paper are the sum of the noise and null space errors, which are calculated following Wunsch et al. (1983) and Rintoul (1991). These errors represent the formal error of the inverse method—the error associated with determining the barotropic velocity and diapycnal fluxes. These formal errors do not account for errors due to the asymptotic data, solution sensitivity to the first guess, and ocean variability. As the formal errors do not include these other error sources, they may not be an accurate reflection of the true uncertainty of the flux estimates.

## *b. Southern Hemisphere large-scale circulation*

The main focus of this paper is on the diapycnal transports. To provide a context for this discussion, we first briefly describe the net meridional and zonal fluxes (Table 3) and a five-layer circulation summary (Table 4).

### 1) SUBTROPICAL ATLANTIC

Across the Atlantic there is a small net southward flux of mass and salt that corresponds to the leakage of Pacific water through Bering Strait and into the North Atlantic Ocean (Table 3). [The slight increase in mass flux between SAVE2 and SAVE4 does not represent a convergence of freshwater but rather is a result of choosing a solution (rank) where the layer residual norms are of  $O[1 \text{ to } 2(\times 10^6 \text{ m}^3 \text{ s}^{-1})]$ ].

The individual layer fluxes show the Atlantic overturning circulation (Table 4). Southward flow of North Atlantic Deep Water is balanced by northward flow of thermocline and intermediate water and Antarctic Bottom Water. The  $-17 \pm 3$  NADW overturning agrees well with previous estimates (Dickson and Brown 1994; Rintoul 1991; McCartney 1993), although it is smaller than the most recent estimates of  $-28 \pm 1$  at  $11^\circ\text{S}$  and  $-20 \pm 1$  at  $23^\circ\text{S}$  (Macdonald 1998). This study and that of Macdonald (1998) both close the NADW overturning by a northward flux of upper water, but the division of the northward transport between warm, salty thermocline water and slightly cooler, fresher intermediate water differs. In this study the northward transport is predominantly achieved by intermediate water while in the earlier study the northward return is equally divided between thermocline and intermediate water.

Compensation of the southward export of NADW by northward flow of upper waters results in a northward heat flux across the Atlantic. In this study we estimate a heat flux of  $0.42 \pm 0.05$  PW at SAVE2 and  $0.28 \pm 0.04$  PW at SAVE4. (All heat fluxes herein are relative to  $0^\circ\text{C}$ .) The increase in the northward heat flux between these sections is due to the addition of heat across the air–sea interface, which is explicitly included in our model. The heat flux is similar to that of Rintoul (1991) but smaller than more recent estimates by Macdonald (1998) of  $0.49 \pm 0.25$  PW and Saunders and King (1995)  $0.5 \pm 0.1$  PW. Both of the previous studies have a larger northward flux of warmer, thermocline water, which explains their larger northward heat flux estimates.

### 2) SUBTROPICAL INDIAN

In the Indian Ocean there is a southward mass flux at  $18^\circ\text{S}$  and  $32^\circ\text{S}$  of  $10.4 \pm 3.1 \times 10^6 \text{ m}^3 \text{ s}^{-1}$  and  $10.3 \pm 2.3 \times 10^6$

$\text{m}^3 \text{s}^{-1}$ , respectively (Table 3). The southward mass flux through the Indian Ocean is within reasonable agreement of recent estimates of the size of the Indonesian Throughflow (Cresswell et al. 1993; Meyers et al. 1995).

The deep overturning circulation of this model is different from recent schemes presented by Toole and Warren (1993), Robbins and Toole (1997), and Macdonald (1998). The two most recent studies show a deep to thermocline overturning circulation of  $12 \pm 3 \times 10^6 \text{ m}^3 \text{ s}^{-1}$  and  $17 \pm 5 \times 10^6 \text{ m}^3 \text{ s}^{-1}$ , respectively. In this study we estimate a stronger overturning circulation of  $23 \pm 3 \times 10^6 \text{ m}^3 \text{ s}^{-1}$ , which is effectively balanced below 1500 dbar (Table 4). Our stronger overturning is similar to the  $27 \times 10^6 \text{ m}^3 \text{ s}^{-1}$  of Toole and Warren (1993), but significantly, their study balances the northward flow by southward thermocline and intermediate water transport above 1500 dbar.

Because the overturning circulation is closed by relatively cool water below 1500 dbar, the heat flux is smaller than other recent studies. We find a southward heat flux at  $32^\circ\text{S}$  of  $-0.87 \pm 0.06 \text{ PW}$ . At the same section Macdonald (1998) estimates  $-1.30 \pm 0.28 \text{ PW}$ , and Toole and Warren (1993) estimate a southward flux of  $-1.67 \text{ PW}$ . [Robbins and Toole (1997) use the same  $32^\circ\text{S}$  section, but they calculate heat divergence north of  $32^\circ\text{S}$ .]

The reduced vertical extent of the overturning circulation in this model results in a smaller silica flux than found by Toole and Warren (1993). The smaller silica flux is more consistent with our current understanding of the World Ocean silica balance, in which the Southern Ocean is estimated to be a silica sink (Truesdell et al. 1995).

### 3) SUBTROPICAL PACIFIC

Across  $32^\circ\text{S}$  in the Pacific Ocean there is a net northward transport of  $7.4 \pm 2 \times 10^6 \text{ m}^3 \text{ s}^{-1}$ . This results from a net northward flux of thermocline layers (Table 4). There is a large northward flux of  $26 \pm 2 \times 10^6 \text{ m}^3 \text{ s}^{-1}$  of lower deep and bottom water into the Pacific Ocean. This is much larger than the  $8 \pm 5 \times 10^6 \text{ m}^3 \text{ s}^{-1}$  estimated by Macdonald (1998), and the  $12 \times 10^6 \text{ m}^3 \text{ s}^{-1}$  estimated by Wunsch et al. (1983) and Tsimplis et al. (1998), but only slightly larger than the early, Warren (1981b)  $20 \times 10^6 \text{ m}^3 \text{ s}^{-1}$  estimate of deep northward flow in the western boundary current.

Table 4 shows that the Pacific and Indian Ocean deep overturning circulations are similar. Northward flowing lower deep and bottom water is converted to slightly less dense Pacific Deep Water, which is returned to the Southern Ocean. The confinement of the deep overturning circulation below 1500 dbar is in agreement with previous studies (Wunsch et al. 1983; Toggweiler and Samuels 1993).

The heat flux is  $0.14 \pm 0.04$  at  $32^\circ\text{S}$ . Macdonald (1998) estimates heat fluxes of  $-0.04 \pm 0.32$  at  $28^\circ\text{S}$  and  $0.26 \pm 0.28$  at  $43^\circ\text{S}$ . The combined southward heat flux at nominally  $35^\circ\text{S}$  (SAVE4, Ind32, and Pac32) is  $-0.46 \pm 0.14 \text{ PW}$ . A similar calculation from Macdonald (1998) (sum of the heat flux across the southern subtropical sections) gives an estimated southward heat flux of  $-0.85 \pm 0.83 \text{ PW}$ .

### 4) SOUTHERN OCEAN

In the Southern Ocean the Antarctic Circumpolar Current (ACC) dominates the three choke point sections with an eastward mass flux of  $134.9 \pm 1 \times 10^6 \text{ m}^3 \text{ s}^{-1}$  at Drake Passage,  $135.4 \pm 3 \times 10^6 \text{ m}^3 \text{ s}^{-1}$  south of Africa, and  $145.6 \pm 1 \times 10^6 \text{ m}^3 \text{ s}^{-1}$  south of Australia (Table 3). These transports are approximately  $5 \times 10^6 \text{ m}^3 \text{ s}^{-1}$  smaller than estimates of Macdonald (1998) at corresponding longitudes. Macdonald constrained the transport of the ACC at Drake Passage to be  $142 \pm 5 \times 10^6 \text{ m}^3 \text{ s}^{-1}$ ; this study has no a priori constraint on the transport of the ACC. Across the Weddell Sea section there is a  $0 \pm 3 \times 10^6 \text{ m}^3 \text{ s}^{-1}$  net mass flux. Underlying the zero mass flux is an overturning circulation that converts  $11 \pm 2 \times 10^6 \text{ m}^3 \text{ s}^{-1}$  of deep (layer 15–19) and lighter bottom water (layer 20) to denser Weddell Sea deep and bottom water (layer 21–23). The net production of  $11 \times 10^6 \text{ m}^3 \text{ s}^{-1}$  of Weddell Sea deep and bottom water agrees with recent estimates (Fahrbach et al. 1994).

Associated with the large eastward mass transport of the ACC are eastward heat, salt, freshwater, and silica fluxes (Table 3). Across the Southern Ocean choke point sections the eastward heat fluxes are  $1.41 \pm 0.01 \text{ PW}$  at Drake Passage,  $1.19 \pm 0.03 \text{ PW}$  south of Africa,  $1.83 \pm 0.01 \text{ PW}$  south of Australia. In the Southern Ocean Atlantic sector there is also a southward flux of  $-0.05 \pm 0.01 \text{ PW}$  into the Weddell Sea. The heat fluxes at Drake Passage and south of Africa are similar to estimates of Macdonald (1998), while south of Australia there is a  $0.10 \text{ PW}$  difference in the estimated heat flux.

The property divergences between the choke point sections result from imports or exports across the three southern subtropical sections and from changes to the water layer composition between the choke point sections (Table 4). The

largest divergences occur south of Africa and south of Australia. The increases in eastward property fluxes south of Australia result from the inclusion of Indonesian Throughflow water in the Indian sector and their eastward transport with the ACC.

### c. Diapycnal fluxes

The summary of the circulation presented above shows that the net fluxes are generally consistent with earlier estimates, where they exist. Here we focus on the diapycnal fluxes required to accomplish the water mass conversions implied by the divergence of the lateral fluxes.

Comparison of  $T$ - $S$  curves at the sections used in the inverse model (see figures referred to below) shows that the  $T$ - $S$  properties for individual layers vary substantially across each ocean basin. The changes in  $T$ - $S$  properties reflect the modification of water masses due to air-sea fluxes and interior mixing. In this section we quantify the interior mixing and demonstrate the consistency between the diapycnal flux estimates and the observed  $T$ - $S$  curves. As we are interested here in quantifying the interior fluxes, we will focus on intermediate and deep water masses (layers 10–23). Focusing on these layers minimizes the effect of interaction between air-sea fluxes and interior mixing.

#### 1) SUBTROPICAL ATLANTIC


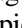
[Figure 2a](#) shows the diapycnal velocity for mass for the subtropical Atlantic (Box I). (Recall that the diapycnal mass fluxes enter the conservation equations in the form of a diapycnal advection, which when multiplied by the interface area gives the net diapycnal mass flux.) In [Fig. 2b](#) the diapycnal mass, heat, and salt fluxes are shown. The largest diapycnal mass velocity occurs across the densest interface. This interface defines the upper boundary of the coldest, freshest Weddell Sea Deep Water (WSDW) that enters the Argentine Basin (with a transport of  $1 \pm 0.5 \times 10^6 \text{ m}^3 \text{ s}^{-1}$  in the inverse model). This layer only occupies a small area of the Argentine Basin just north of the Scotia Ridge. The small area occupied by this water mass and the requirement that this water is modified to slightly less dense AABW results in the large interface velocity.

North Atlantic Deep Water and Circumpolar Deep Water occupy the same density range corresponding to layers 15–18. Intermediate water [subantarctic mode water (SAMW) and Antarctic Intermediate Water (AAIW)] occupies layers 10 to 14, with the salinity minimum lying in layer 14. The mass and heat fluxes are upward across interfaces 16 to 14. The upward heat flux from NADW into intermediate water is up the temperature gradient because the advective heat flux is larger than the downward diffusive flux. The salt diapycnal fluxes are upward across NADW (18 to 16), resulting in a salt flux from NADW into low salinity intermediate water (14 and 15). Across the upper intermediate interfaces (layers 10 to 14) the mass flux is upward and small while the heat and salt fluxes are downward. Across these layers (10 to 14) there is a downward flux of heat and salt from overlying warmer, saltier subtropical Atlantic thermocline water into cooler, fresher intermediate water. The layers most affected by the downward heat and salt fluxes from overlying thermocline water are the upper intermediate layers, which correspond to SAMW (layers 10 to 12).


These diapycnal fluxes result in substantial modification of water masses in the subtropical Atlantic. Mixing with cold, fresh AABW and CDW from the Southern Ocean and lateral or isopycnal mixing particularly in layer 17 [neutral density ( $\sigma^{\theta}$ ) 27.8–28.0] can explain the changes in  $T$ - $S$  characteristics of the NADW core between SAVE2 ( $2.5^{\circ} \leq \theta \leq 3.5^{\circ}$  and  $S \geq 34.9$ ) and SAVE4, where the core of NADW crosses the Mid-Atlantic Ridge and enters the Southern Ocean ( $1^{\circ} \leq \theta \leq 3^{\circ}\text{C}$  and  $S \geq 34.7$  psu) ([Fig. 3](#)). The diapycnal fluxes that cool and freshen the NADW at its lower boundary and freshen it at its upper boundary may also explain the shift of NADW core extrema to higher densities as it moves southward in the South Atlantic ([Reid 1989](#)).



[Schmitz \(1995\)](#), [Schmitz \(1996\)](#), and [Talley \(1996\)](#) describe the substantial changes in the  $T$ - $S$  characteristics of intermediate water as it crosses the South Atlantic. They highlight the warming and salinification of intermediate water in the southwest Atlantic, and [Schmitz \(1996\)](#) points out the salinity increase of upper intermediate water (his UPIW) between Drake Passage and  $25^{\circ}\text{W}$ . The downward diapycnal fluxes of heat and salt from the overlying thermocline water described here account for the warming and increased salinity of AAIW. Although the fluxes here describe a “box” mean diapycnal flux from the thermocline to the intermediate layers, the most likely site for this mixing between subtropical thermocline water and AAIW is in the Brazil–Malvinas confluence zone in the western Atlantic between  $33^{\circ}\text{S}$  and  $38^{\circ}\text{S}$ . The inverse model solution maintains the northward extension of the ACC along the coast of South America (the Malvinas Current) included in the initial guess. [Figure 4](#) shows the  $T$ - $S$  plots for SAMW and AAIW in Drake Passage, the Malvinas Current, and at SAVE4 over the Mid-Atlantic Ridge and in the Angola and Cape Basins. This highlights the warming and salinity increase of SAMW/AAIW occurring in the subtropical Atlantic. The greatest temperature and salinity changes occur in the western basins between the Drake Passage–Malvinas extension and the Mid-Atlantic Ridge. Intermediate water that enters via Drake Passage moves northward in the Malvinas Current until it collides with the southward flowing Brazil Current. At this confluence the subtropical water in the Brazil Current overrides the denser AAIW. The confluence of these water masses results in the downward heat and salt fluxes shown. The smaller differences in the  $T$ - $S$  profile between the

## 2) SUBTROPICAL INDIAN

The diapycnal mass velocity and diapycnal mass, heat, and salt fluxes for the Indian Ocean between 32°S and 18°S (Box IV) are shown in [Fig. 5](#) . The magnitude of the diapycnal mass velocity across the densest layer are approximately three times larger than those in the subtropical Atlantic ([Fig. 2](#) ). The large velocity across the upper boundary of AABW again reflect the modification of AABW to CDW within the subtropical Indian Ocean. At 32°S  $10 \pm 0.85 \times 10^6 \text{ m}^3 \text{ s}^{-1}$  of AABW (layer 20) enters the subtropical Indian Ocean from the south; at 18°S only  $1 \pm 0.04 \times 10^6 \text{ m}^3 \text{ s}^{-1}$  of AABW move northward in the western Madagascar Basin, while a total of  $6 \pm 3 \times 10^6 \text{ m}^3 \text{ s}^{-1}$  (layer 19) of LCDW moves north in the Western Australian and Madagascar Basins. Apart from the conversion of AABW to LCDW, there is an upward velocity from LCDW (layer 19 to 18) to overlying deep layers that results in a conversion of LCDW into UCDW and IDW (layers 17 to 15). The upward property fluxes from the AABW and LCDW are confined to below layer 15, which is the upper boundary of southward flowing UCDW and IDW. The net result of the upward diapycnal property fluxes is that  $16 \pm 2 \times 10^6 \text{ m}^3 \text{ s}^{-1}$  of the  $23 \pm 3 \times 10^6 \text{ m}^3 \text{ s}^{-1}$  of AABW and CDW that flow northward across 32°S are converted to slightly less dense UCDW and IDW, while the remaining  $7 \pm 2 \times 10^6 \text{ m}^3 \text{ s}^{-1}$  moves northward across 18°S where it is further modified to become IDW and thermocline water.

The diapycnal mass fluxes found here differ from those of [Robbins and Toole \(1997\)](#) and [Schmitz \(1996\)](#): his Fig. II-129), which is heavily influenced by the work of [Robbins and Toole \(1997\)](#), but are similar to the circulation pattern described in [Schmitz \(1996\)](#): Fig. II-156). The main differences relate to the size of the overturning circulation and the strength and structure of the diapycnal velocities. [Robbins and Toole \(1997\)](#) estimate an inflow of  $13 \times 10^6 \text{ m}^3 \text{ s}^{-1}$  of deep and bottom water across 32°S, which supplies more or less uniform upwelling to 500 dbar. Their meridional overturning cell results in a conversion of AABW and LCDW into thermocline and surface water. Our solution shows a vertical cell that is confined below 1500 dbar and results in the conversion of  $13 \pm 2 \times 10^6 \text{ m}^3 \text{ s}^{-1}$  of AABW and LCDW into UCDW and IDW. There is an implied further conversion ( $7 \times 10^6 \text{ m}^3 \text{ s}^{-1}$ ) of LCDW to IDW and thermocline water north of 18°S. The diapycnal mass velocities are large [ $O(10^{-6} \text{ m s}^{-1})$ ] but recent work by [Polzin et al. \(1997\)](#) shows enhanced vertical mixing over rough topography. The Indian Ocean is divided into numerous small basins by topographic ridges and plateaus. These topographic features may act to enhance mixing and result in the large diapycnal velocities found in this study.

Layer 14 ([Fig. 5](#) ) marks the boundary between bottom and deep layers (19 to 15) and intermediate and thermocline water (14 to 3) and also a significant change in the sign of the diapycnal mass velocity and property fluxes. There is a downward flux of heat from warm surface and thermocline layers (3 to 10) into cooler SAMW and AAIW, which acts to warm these intermediate waters as they circulate in the subtropical gyre. There is a strong divergence of salt across layers 11 and 12. The downward flux of salt into intermediate waters (12 to 14) increases the salinity of SAMW and AAIW in the Indian subtropical gyre, while the upward flux of salt into thermocline layers enhances the subsurface salinity maximum that develops between 32°S and 18°S. The subsurface salinity maximum between 32°S and 18°S is thought to result from excess evaporation over the subtropical Indian Ocean ([Warren 1981a](#); [Toole and Warren 1993](#)). As this layer moves northward, it is capped by fresher surface water that originates as Indonesian Throughflow water and fresher surface waters of the northern Indian Ocean, while below the layer lies fresher SAMW and AAIW. The combined effect of downward heat flux from surface and upper thermocline layer into intermediate SAMW/AAIW and the salt divergence from layer 11 results in the small downward mass velocities and associated fluxes from surface and upper thermocline waters into lower thermocline and intermediate waters.

The changes in temperature and salinity of SAMW and AAIW as they circulate in the subtropical gyre can be illustrated by comparing the properties of AAIW and SAMW between the eastern and western basins at 32°S. Newly ventilated SAMW and AAIW from the Southern Ocean enter the Indian Ocean in the eastern Crozet, Central, and Perth Basins, and return southward in the western Natal, Mozambique, and Madagascar basins ([Fig. 6](#) ). The SAMW and AAIW warm and increase in salinity as they circulate around the subtropical gyre, with the largest salinity increases occurring within SAMW ( $\gamma^s$  26.0–27.0). These changes to the characteristics of SAMW and AAIW in the Indian subtropical gyre are the result of the diapycnal fluxes shown in [Fig. 5](#) .

## 3) SOUTHERN OCEAN ATLANTIC SECTOR

The Southern Ocean is dominated by the strong eastward Antarctic Circumpolar Current. Interactions of the ACC with the adjacent basins to the north and production of extreme AABW near the Antarctic continent result in significant changes to property and volume fluxes of individual water masses. For example, in the Atlantic sector of the Southern Ocean (Box II) CDW (LCDW and UCDW) is carried eastward through Drake Passage as part of the ACC. Some deep water is cooled in the Weddell Sea, resulting in a net transfer of LCDW to Weddell Sea Deep Water and Weddell Sea Bottom Water. Across the northern boundary, northward flow of AABW, intermediate, and thermocline water is balanced by modified NADW flowing



to the south. The addition of WSDW, WSBW, and NADW in the Atlantic sector results in major changes in the transport and properties of AABW, LCDW, and UCDW between Drake Passage and the exit of the ACC south of Africa. [Figure 7](#) shows the diapycnal mass velocity and property fluxes for the Southern Ocean Atlantic sector. Across the deepest layers (21 and 20), which identify WSDW and WSBW, there is a downward heat flux from overlying warmer LCDW. The downward flux of heat from AABW and LCDW into WSDW and WSBW warms these extreme bottom-water masses and results in their conversion to less extreme AABW, which is then able to move northward into the Argentine Basin and eastward with the ACC south of Africa. The upward salt flux from WSDW and WSBW opposes the salt gradient but results because the upward advective salt flux is larger than the downward diffusive flux. In this sector the inflowing NADW is defined between layers 18 to 16 and its associated salinity maximum is within layers 17 and 16. These layers are coincident with both UCDW and LCDW within the ACC. Across CDW and NADW layers there is a downward flux of heat into AABW. There is also a small downward salt flux from NADW (16 and 17). The downward heat and salt fluxes from CDW and NADW into AABW result in an upward mass flux of AABW into the lower CDW (layer 18 and 19). The salt flux from NADW to LCDW results in an increase in the salinity of LCDW and an erosion of the salinity maximum of NADW.

The effect of these diapycnal fluxes in the Southern Ocean Atlantic sector is clearly evident when comparing  $T-S$  characteristics between Drake Passage, south of Africa and SAVE4 ([Fig. 4](#)). CDW that enters through Drake Passage shows only a weak salinity maximum identifying LCDW, but the lighter, lower salinity UCDW is prominent. The high salinity NADW entering the Southern Ocean over the Mid-Atlantic Ridge on SAVE4 is in the same density range as the CDW. Cold, fresh WSDW from the Weddell Sea is also added in the Atlantic sector and mixes with LCDW to form AABW. The addition of NADW and new AABW contribute to the change in the  $T-S$  curve between Drake Passage and south of Africa. The temperature and salinity characteristics south of Africa show cold, fresh AABW leaving with the ACC, as well as the very high salinity NADW supplied from the Atlantic. Mixing between the AABW and the salinity maximum water within the South Atlantic forms deep water with intermediate properties, which is exported to the Indian Ocean. The diapycnal mixing between WSDW, AABW, CDW, and NADW (and isopycnal mixing between CDW and NADW) quantified in this study explains the changes in the  $T-S$  curves in the Southern Ocean Atlantic sector.

Across the thermocline and SAMW (10 and 11) layers there is a downward flux of heat and salt into lower SAMW and AAIW (12 to 14) and also a small upward salt flux from NADW. These salt and heat fluxes from overlying thermocline and warmer, saltier SAMW result in a mass flux from upper intermediate waters into lower intermediate water. This mixing occurs in the northeastern region of the Southern Ocean Atlantic sector and is associated with the bifurcation of the South Atlantic Current (SAC) where a portion feeds directly into the Benguela Current while the remainder returns to the sector, south of Africa, after a sojourn in the southeast Indian Ocean ([Stramma and Peterson 1990](#); [Gordon et al. 1992](#)). The SAMW returning to the Atlantic south of Africa is slightly warmer and saltier than modified SAMW, which flows eastward over the Mid-Atlantic Ridge. The diapycnal and isopycnal mixing of thermocline water and warmer, saltier SAMW with cooler, fresher SAMW and AAIW in this region result in the warmer, saltier AAIW seen in the Angola and Cape Basins ([Fig. 4](#)).

#### 4) SOUTHERN OCEAN INDIAN SECTOR

The ACC south of Africa, following interactions in the Southern Ocean Atlantic sector, is made up of cold AABW, a salinity maximum LCDW, lower salinity UCDW, salinity minimum AAIW, and SAMW. In the Southern Ocean Indian sector (Box V) there are exchanges of AABW and LCDW with UCDW and IDW across 32°S and a net inflow of Indian thermocline water and intermediate water originating in the Indonesian Throughflow. On the southern boundary with the Antarctic continent previous studies have identified production of AABW at Adélie Land ([Rintoul 1998](#)) and Prydz Bay ([Wong et al. 1998](#)). Production of extreme bottom water requires the conversion of LCDW and AABW into these denser layers. As this newly formed bottom water moves northward and eastward with the ACC, it mixes with overlying AABW and LCDW resulting in a net production of warmer, saltier AABW and cooler, fresher LCDW. These modified water masses then flow eastward with the ACC south of Australia and northward across 32°S.

The LCDW lost to mixing with and production of AABW, as well as the northward flux of AABW and LCDW at 32°S, is balanced by a southward flux of UCDW and IDW across 32°S and subsequent conversion to denser layers within the Southern Ocean. These mixing processes require downward diapycnal property fluxes from UCDW and IDW to LCDW and AABW layers. [Figure 8](#) shows downward diapycnal mass velocity and property fluxes from UCDW (layer 15) to the densest layer corresponding to LCDW and AABW. The downward flux of slightly fresher, warmer UCDW into LCDW and the input of new cold AABW in this region and isopycnal mixing are highlighted by the difference in the  $T-S$  diagrams between Africa and Australia ([Fig. 9](#)). The flux of UCDW into LCDW results in the erosion of the salinity maximum while the influence of AABW produced in the Indian sector slightly increases the salinity of the densest water, and further erodes the salinity maximum of the overlying LCDW.

[Figure 8](#) shows significant downward heat and salt fluxes from the thermocline (layers 10 and above) into SAMW and AAIW (11 to 14). The downward diapycnal fluxes from thermocline waters probably occur in the northwestern corner of the box as warm, salty Indian thermocline water extends southward with the Agulhas Current and meets cool, fresh Southern Ocean waters. However, the evolution of the  $T-S$  properties of SAMW in the South Indian Ocean is not due solely

to “interior” mixing. The SAMW cools and freshens across the Indian Ocean due to air–sea exchange ([McCartney 1977](#); [Sloyan 1997](#); Sloyan and Rintoul 2000, manuscript submitted to *J. Phys. Oceanogr.*). The heat and salt provided by diapycnal fluxes is apparently more than compensated by cooling and freshening by the atmosphere.

## 5) SOUTHERN OCEAN PACIFIC SECTOR

As in the Indian sector, the Pacific sector is known to be a source of AABW (e.g., [Jacobs et al. 1985](#); [Carmack 1990](#); [Rintoul 1998](#)), and we again lack a section near the Antarctic coast to isolate the bottom water production regions. Interactions between UCDW, LCDW, AABW, and newly formed Ross Sea Bottom Water (RSBW) and ALBW in the Pacific sector are similar to those described for the Indian sector. In the Pacific sector there is also northward flow of AABW and LCDW and balancing southward flow of UCDW and PDW across 32°S. The production of new RSBW and ALBW, its subsequent modification to less extreme AABW by mixing with overlying LCDW, and the replacement of northward flowing AABW and LCDW by UCDW and PDW across 32°S would result in downward diapycnal property fluxes between these water masses as shown in [Fig. 10](#). [Figure 9](#) shows how downward mixing of warmer, fresher UCDW and PDW into LCDW and isopycnal mixing in LCDW further erodes the salinity maximum between Australia and Drake Passage.

The diapycnal property fluxes redistribute mass, heat, and salt within the intermediate layers (11 to 14) ([Fig. 10](#)). There is a downward flux of heat and salt from overlying thermocline layers (10) but little mass flux. As in the Indian sector, the SAMW cools and freshens across the Pacific, largely due to air–sea exchange. The diapycnal fluxes in this sector act to make the SAMW and AAIW warmer and saltier, a tendency which is more than compensated by the air–sea exchange. A discussion of the role of air–sea fluxes in driving SAMW and AAIW formation is contained in a subsequent paper.

## 5. Discussion

The physical interpretation of the Southern Ocean heat and salt diapycnal fluxes describe the mixing occurring between water masses within box regions that result in the changes to the  $T$ – $S$  properties at the bounding hydrographic sections. When describing the mass, temperature, and salt fluxes occurring across diapycnal surfaces there are numerous examples where either the heat or salt diapycnal fluxes, or both, opposes the mass flux ([Figs. 2](#), [5](#), [7](#), [8](#), and [10](#)). The breakdown of the total heat and salt diapycnal flux for the subtropical Atlantic (Box I) into the mean advective flux ( $Aw_m^* \bar{C}$ , where  $A$  is the area of isopycnal,  $w_m^*$  is the mean advection given by the mass diapycnal velocity, and  $\bar{C}$  is the mean isopycnal tracer concentration) and diffusion/eddy flux is shown in [Fig. 11](#). The figure shows those layers where diffusion and eddy processes make a significant contribution to the net diapycnal flux, so the mean advective flux ( $Aw_m^* \bar{C}$ ) is not a good representation of the net diapycnal flux.

For the Southern Ocean sectors there appears to be better agreement of the mass, heat, and salt diapycnal fluxes, particular in the deep layers (15 to 19). [Figure 12](#) show a similar breakdown of the total diapycnal heat and salt fluxes for the Southern Ocean Indian sector into its mean advection and diffusion/eddy components for the Southern Ocean Indian sector. Across the intermediate layers (10 to 14) the diffusion and eddy fluxes still make significant contributions to the total diapycnal heat and salt fluxes. The contribution of the diffusion and eddy flux in the deep layers is not so dramatic but they provide small adjustments to the mean advective flux.

The layers in [Figs. 11](#) and [12](#) where the diffusion and eddy diapycnal fluxes make significant contributions to the total heat or salt diapycnal flux correspond to those that outcrop (e.g., layers 10 to 17) and those that intersect regions of energetic eddy mixing in the Brazil–Malvinas Confluence zone and Agulhas Retroflexion (layers 10 to 14). This correspondence is similar to that found in the FRAM study (see the appendix). The inversion with real ocean data supports the finding that the “eddy” ( $\overline{e'c'}$ ) contribution is large in some locations, and ignoring it (e.g., by representing the net diapycnal flux as a mean advective flux) is likely to degrade estimates of both lateral and diapycnal fluxes.

[Macdonald \(1998\)](#), in a recent global inverse model, parameterizes property diapycnal fluxes as  $Aw_m^* \bar{C}$ . She finds that diapycnal terms are generally small and in some regions exhibit a random character. A comparison of the direction of the diapycnal property fluxes between her study and ours shows the property diapycnal fluxes across the deepest layers in the Southern Ocean sectors generally agree. In these deep layers, diapycnal fluxes of mass, heat, and salt are directed toward denser layers. In our study, diapycnal fluxes of mass, heat, and salt in intermediate layers can be opposed, while the parameterization used by Macdonald requires all property fluxes to be of the same sign.

In the subtropical Atlantic and Indian Oceans significant differences in the diapycnal fluxes exist between our study and [Macdonald \(1998\)](#). In Macdonald the diapycnal property fluxes in the subtropical Atlantic and Indian regions generally alternate between upwelling across the deepest layers below 4000 dbar, downwelling between 4000 and 3000 dbar and upwelling above 3000 dbar. In the subtropical Atlantic we show an upward diapycnal mass flux across all layers, while the

heat and salt diapycnal fluxes are downward in the intermediate and deep layers. In the subtropical Indian region the upward diapycnal mass flux in bottom and deep layers to 1500 dbar is opposed by downward heat and salt fluxes (Fig. 11).

Macdonald (1998) shows that in the Agulhas Retroflection and southeastern South Atlantic the diapycnal fluxes have a random structure. These regions are sites of high eddy variability. Our results suggest that it is precisely in these regions where an  $Aw_m^* \bar{C}$  parameterization of the diapycnal property fluxes is not appropriate.

Comparison of the diapycnal property fluxes between each box shows that both the subtropical Atlantic (Fig. 2) and subtropical Indian (Fig. 5) have upward mass fluxes across the bottom and deep layers (20 to 15). The subtropical regions are converting these bottom and lower deep waters to less dense upper deep water. The size of the diapycnal mass velocity across the deepest layers is  $2 \times 10^{-6} \text{ m s}^{-1}$  for the subtropical Atlantic and  $6 \times 10^{-6} \text{ m s}^{-1}$  for the subtropical Indian. Both regions show a decrease in the size of the diapycnal velocity in overlying deep layers. The pattern of upwelling of bottom and deep water to less dense water in the subtropical region is similar, but the upwelling is much stronger in the Indian Ocean. Published estimates of vertical velocity for the subtropical Atlantic between 30°S and 11°S between 3200 and 4000 dbar (layers 18 and 19) range from  $3.1 \times 10^{-7}$  to  $8 \times 10^{-7} \text{ m s}^{-1}$  (Warren and Speer 1991; Speer and Zenk 1993). In this study the diapycnal velocity across layers 18 and 19 is  $2 \times 10^{-7}$  and  $5 \times 10^{-7} \text{ m s}^{-1}$ , respectively. In the subtropical Indian Ocean estimates vary from between  $4 \times 10^{-7}$  and  $7 \times 10^{-7} \text{ m s}^{-1}$  at 2000 dbar (Warren 1981a; Toole and Warren 1993; Robbins and Toole 1997) while at a similar depth (layer 17) the estimated diapycnal velocity in this study is  $2 \times 10^{-6} \text{ m s}^{-1}$ . Our diapycnal velocity estimates for the subtropical Atlantic region are similar to the earlier estimates, but our values for the subtropical Indian Ocean are somewhat larger than previous estimates. The difference in the diapycnal velocity for the Indian Ocean between this study and previous studies relates to the differences in the circulation pattern, as explained above. Across the intermediate layers (10 to 14) the subtropical Atlantic diapycnal velocity is upward, while in the Indian Ocean it is downward. The magnitude of the velocities are similar. The difference in the direction of the fluxes across the intermediate layers suggests different mixing mechanisms between intermediate and thermocline water in the subtropical Atlantic and Indian Oceans.

The larger diapycnal mass fluxes in the Indian Ocean may be the result of the complicated bathymetry in that basin relative to the Atlantic. The topography of the Indian Ocean provides many more avenues for the existence of strong northward bottom and deep western boundary currents through its numerous deep basins (Madagascar, Mascarene, Crozet, and Perth basins). In contrast bottom and deep water can only move northward into the subtropical Atlantic in the western Argentine basins as the eastern basin is closed by the Walvis Ridge. As the numerous ridges and plateaus in the Indian Ocean act to channel and intensify the northward flow of bottom and deep water, they may also provide the mechanism for enhanced diapycnal mixing (Wunsch 1970; Armi 1978; Polzin et al. 1997).

The Southern Ocean sectors (Figs. 7, 8, 10) have downward (toward higher density) mass velocity and fluxes across the deep layers (15 to 18), with mean values of  $2 \times 10^{-7}$  (Atlantic),  $5 \times 10^{-7}$  (Indian), and  $6 \times 10^{-7} \text{ m s}^{-1}$  (Pacific). Across the bottom and LCDW layers (19 to 22) the Atlantic sector has upward diapycnal mass fluxes while in the Indian and Pacific sector the flux is downward. The difference in sign of the diapycnal mass flux in the Atlantic relates to the presence of the Weddell Sea section, which separates the waters near Antarctica from the interior of the Atlantic sector. The inclusion of the Weddell Sea section enables the conversion of CDW to WSDW and WSBW taking place in the Weddell Sea to be isolated from the diapycnal fluxes in the interior, where entrainment and mixing convert WSBW/WSDW to less dense AABW. The downward fluxes across deep and bottom layers in the Indian and Pacific sectors reflects the production of ALBW and RSBW. These waters subsequently mix with overlying CDW to increase the volume of AABW in these regions, but the net diapycnal flux remains downward. In all three basins a consistent pattern is found: formation of dense water near Antarctica, and erosion by entrainment of lighter water away from the continent. The circumpolar nature of isopycnals in the Southern Ocean does not readily allow estimates of diapycnal velocities as provided for the northern subtropical basins (where these estimates are generally given for cul-de-sac isopycnals where the lateral input flux is known). Thus for the Southern Ocean there are no previous estimates of vertical velocity available to compare our results with.

The intermediate layers also have downward diapycnal mass fluxes in all regions, apart from the subtropical Atlantic (Box I). In the Southern Ocean Indian and Pacific sectors the evolution of intermediate water is not solely determined by “interior” mixing. In these regions the interaction of “interior” mixing and air-sea fluxes plays a major role in the production and modification of intermediate water.

The diapycnal fluxes quantified in this study result from the divergence in density layers between the hydrographic sections that bound each box. To evaluate the significance of the inferred diapycnal fluxes, we need to address the question of whether the “signal” associated with real diapycnal fluxes in the ocean can be distinguished from the “noise” introduced by temporal variability, given that we combine asynoptic sections. The section-to-section divergence in density layers, over the large spatial scales of the boxes used in this study, is primarily related to the overturning circulation; for example,

southward transport of NADW must be balanced by northward flow in a different density class, and AABW/LCDW flowing north into the subtropical basins must return to the Southern Ocean as a lighter water mass, which in turn is involved in the production of AABW near the Antarctic margin. That is, the existence of a mean overturning circulation implies a need for diapycnal fluxes of sufficient magnitude to close the overturning cells. Since the overturning circulation is a robust aspect of the mean circulation, which is likely to be present in any synoptic realization, the diapycnal fluxes are unlikely to be dominated by noise due to temporal variability. Moreover, the influence of diapycnal fluxes is also shown by the systematic evolution of water mass properties across the ocean basins. For example, the salinity of NADW entering the Southern Ocean in the Atlantic section is gradually eroded as it moves eastward with the ACC, while underlying AABW becomes warmer and saltier. The  $T$ - $S$  curves shown here document similar systematic evolution of the  $T$ - $S$  properties in other water masses. These signals are robust features of the mean circulation, which reflect the action of diapycnal fluxes and are present in any synoptic realization of the bounding sections. These facts, together with the overall consistency of our circulation estimates with water properties and previous ocean flux estimates, lead us to conclude that our diapycnal flux estimates are not dominated by noise introduced by the temporal variability.

The balance of these deep-water masses by water in a different density class requires a diapycnal flux, a mean overturning circulation must have a mean diapycnal flux of the same size. In our analysis of the lateral transports and diapycnal fluxes we have placed particular emphasis on the water mass layers such that the lateral and diapycnal property fluxes of the layer is in agreement with independent information (i.e., current moorings),  $T$ - $S$  evolution of the water mass in each region, the vertical property distributions, and consistent with other estimates of these transport reported in the literature. This consistency check is described at great length in the paper. Thus we infer that the three-dimensional circulation is consistent with the mean large-scale circulation and changes in water mass properties within each basin.

We emphasize that the area-averaged diapycnal fluxes vary with depth and in different regions: uniform upwelling from the deep ocean to the thermocline, as assumed in the [Stommel and Arons \(1960\)](#) theory of deep ocean circulation, is not consistent with these results. In particular, the deep meridional overturning inferred in the subtropical Indian and Pacific Oceans is confined below 1500 dbar. The deep overturning found here is consistent with earlier studies in the Pacific ([Wunsch et al. 1983](#); [Tsimplis et al. 1998](#)) and in both basins is consistent with the radiocarbon distribution ([Toggweiler and Samuels 1993](#)), although our Indian Ocean overturning cell differs from recent studies of [Toole and Warren \(1993\)](#) and [Robbins and Toole \(1997\)](#), as discussed above. That the meridional overturning is confined below 1500 dbar has significant implications for the role of the Pacific and Indian interbasin exchange in the global thermohaline circulation ([Sloyan and Rintoul 2000](#)).

## 6. Conclusions

Diapycnal fluxes are an essential element of the global ocean circulation. However, our knowledge of the magnitude and spatial pattern of diapycnal fluxes in the ocean is limited, primarily because they are too weak to observe directly. The purpose of this paper is to explore whether a suitably designed box inverse model can determine area-averaged diapycnal fluxes from basin-scale budgets, with a particular focus on the Southern Ocean.

The structure of the diapycnal fluxes differs between the subtropical (Atlantic and Indian) and Southern Ocean regions. In the subtropical regions, bottom and deep water upwell into less dense water. A more detailed comparison of the subtropical Atlantic and Indian Oceans shows marked differences in the strength and vertical extent of the overturning circulation. The Indian is found to have a much more vigorous overturning circulation that is confined below 1500 dbar and converts AABW and LCDW into less dense UCDW and IDW. The subtropical Atlantic maintains a smaller but constant upwelling to 700 dbar, in which AABW and LCDW mix with less dense NADW and upper NADW mixes with the overlying AAIW.

The diapycnal fluxes across the intermediate layers have different signs in the subtropical Atlantic and Indian basins. In the subtropical Atlantic, lower intermediate water is converted to upper intermediate water and thermocline water, which moves northward in the North Atlantic to close the NADW thermohaline circulation. This conversion of intermediate water to thermocline water is not found in the subtropical Indian Ocean. In the Indian Ocean thermocline water is converted into denser upper intermediate waters. Downward heat and salt fluxes from thermocline to intermediate water in the subtropical Indian Ocean results in progressively warmer and saltier subantarctic mode water as it circulates in the subtropical gyre.

Deep water is converted to denser deep and bottom water in each of the Southern Oceans sectors. The major differences in the diapycnal fluxes between the Southern Ocean sectors occurs across the intermediate layers. In the Indian and Pacific sectors, downward heat and salt fluxes from thermocline water increase the temperature and salinity of SAMW and AAIW. The  $T$ - $S$  properties show that this warming and increased salinity is more than compensated by air-sea interaction in the Indian and Pacific Polar Front and subantarctic zones. The evolution of intermediate waters is not solely driven by “interior” mixing: air-sea fluxes must also be considered to account for the production and modification of SAMW and AAIW in these basins. [Sloyan and Rintoul \(2000\)](#), [Sloyan and Rintoul 2000](#), manuscript submitted to *J. Phys. Oceanogr.*) describe the relative roles of air-sea fluxes and interior mixing in the formation and modification of water masses in the Southern Ocean.

This study demonstrates the feasibility of using hydrographic sections and budget constraints to determine diapycnal

fluxes. The application of similar techniques to the high quality grid of sections collected during WOCE promises to provide, for the first time, a map of the global distribution of diapycnal fluxes. Such a map will be an important step toward a complete understanding of the three-dimensional circulation of the ocean.

### Acknowledgments

We thank Peter McIntosh for his help with the FRAM inverse model, Phil Morgan for writing the Dobox code, and David Webb and Beverly de Cuevas for providing the FRAM output. Comments from Trevor McDougall, Peter McIntosh, and two reviewers improved the manuscript. B. Sloyan was supported by an Australian Postgraduate Award and an Antarctic CRC Ph.D. scholarship. This work contributes to CSIRO's Climate Change Research Program and to the World Ocean Circulation Experiment.

---

### REFERENCES

- Armi, L., 1978: Some evidence for boundary mixing in the deep ocean. *J. Geophys. Res.*, **83**, 1971–1979.
- Budd, W. F., P. A. Reid, and L. J. Minty, 1995: Antarctic moisture flux and net accumulation from global atmospheric analyses. *Ann. Glaciol.*, **21**, 149–156.
- Carmack, E. C., 1990: Large scale physical oceanography of polar oceans. *Polar Oceanography Part A: Physical Science*, W. O. Smith Jr., Ed., Academic Press, 171–222.
- Coachman, L., and K. Aagaard, 1988: Transport through Bering Strait: Annual and interannual variability. *J. Geophys. Res.*, **93**, 15535–15539.
- Cresswell, G. R., A. Frische, J. Peterson, and D. Quadfasel, 1993: Circulation in the Timor Sea. *J. Geophys. Res.*, **98**, 14379–14389.
- da Silva, A. M., C. C. Young, and S. Levitus, 1994: *Atlas of Surface Marine Data 1994*. Vol. 1: *Algorithms and Procedures*, NOAA NESDIS Tech. Rep. 6, U.S. Department of Commerce, 83 pp.
- Dickson, R. R., and J. Brown, 1994: The production of North Atlantic Deep Water: Sources, rates and pathways. *Geophys. Res.*, **99**, 12319–12341.
- Döös, K., and A. Coward, 1997: The Southern Ocean as the major upwelling zone of North Atlantic Deep Water. *Int. WOCE Newslett.*, **27**, 3–4.
- Fahrbach, E., G. Rohardt, M. Schröder, and V. Strass, 1994: Transport and structure of the Weddell Sea. *Ann. Geophys.*, **12**, 840–855.
- Fu, L.-L., 1986: Mass, heat and freshwater fluxes in the south Indian Ocean. *J. Phys. Oceanogr.*, **16**, 1683–1693.
- Gordon, A. L., 1986: Interocean exchange of thermocline water. *J. Geophys. Res.*, **91**, 5037–5046.
- , and B. A. Huber, 1990: Southern Ocean winter mixed layer. *J. Geophys. Res.*, **95**, 11655–11672.
- , R. F. Weiss, W. M. Smethie Jr., and M. J. Warner, 1992: Thermocline and intermediate water communication between the South Atlantic and Indian Oceans. *J. Geophys. Res.*, **97**, 7223–7240.
- Hellerman, S., and M. Rosenstein, 1983: Normal monthly wind stress over the world ocean with error estimates. *J. Phys. Oceanogr.*, **13**, 1093–1104.
- Hogg, N., 1987: A least-squares fit of the advective–diffusive equations to Levitus atlas data. *J. Mar. Res.*, **45**, 347–375.
- , P. Biscaye, W. Gardner, and W. J. Schmitz Jr., 1982: On the transport and modification of Antarctic Bottom Water in the Vema Channel. *J. Mar. Res.*, **40**, 231–263.
- Jackett, D., and T. J. McDougall, 1997: A neutral density variable for the world's oceans. *J. Phys. Oceanogr.*, **27**, 237–263.
- Jacobs, S. S., R. G. Fairbanks, and Y. Horibe, 1985: Origin and evolution of water masses near the Antarctic continental margin. *Oceanology of the Antarctic Continental Shelf*, S. S. Jacob, Ed., Vol. 43, Antarctic Research Series, Amer. Geophys. Union, 59–85.
- Lanczos, C., 1961: *Linear Differential Operators*. Van Nostrand, 564 pp.
- Levitus, S., and T. Boyer, 1994: *World Ocean Atlas 1994*. NOAA Tech. Rep. Atlas NESDIS 4, 117 pp.

- Macdonald, A., 1991: Mass, heat, oxygen and nutrient fluxes at 30°S and their implication for the Pacific–Indian through flow and the global heat budget. M.S. thesis, Woods Hole Oceanographic Institute, Massachusetts Institute of Technology, 183 pp. [Available from Woods Hole Oceanographic Institute, Woods Hole, MA 02543].
- , 1998: The global ocean circulation: a hydrographic estimate and regional analysis. *Progress in Oceanography*, Vol. 41, Pergamon, 281–382.
- McCartney, M. S., 1977: Subantarctic Mode Water. *Deep-Sea Res.*, **24**, 103–119.
- , 1993: Crossing of the equator by the deep western boundary current in the western Atlantic Ocean. *J. Phys. Oceanogr.*, **23**, 1953–1974.
- McIntosh, P. C., and S. R. Rintoul, 1997: Do box inverse models work? *J. Phys. Oceanogr.*, **27**, 291–208.
- Meyers, G., R. J. Bailey, and A. P. Worby, 1995: Geostrophic transport of Indonesian throughflow. *Deep-Sea Res.*, **42**, 1163–1174.
- Peterson, R., 1992: The boundary currents in the western Argentine basin. *Deep-Sea Res.*, **39**, 623–644.
- , and T. Whitworth III., 1989: The Subantarctic and Polar fronts in relation to deep water masses through the southwestern Atlantic. *J. Geophys. Res.*, **94**, 10817–10838.
- , and L. Stramma, 1991: Upper-level circulation in the South Atlantic Ocean. *Progress in Oceanography*, Vol. 26, Pergamon, 1–73.
- Polzin, K. L., J. M. Toole, J. R. Ledwell, and R. W. Schmitt, 1997: Spatial variability of turbulent mixing in the abyssal ocean. *Science*, **276**, 93–96.
- Reid, J. L., 1989: On the total geostrophic circulation of the South Atlantic Ocean: Flow patterns, tracers and transports. *Progress in Oceanography*, Vol. 23, Pergamon, 149–244.
- Rintoul, S. R., 1991: South Atlantic interbasin exchange. *J. Geophys. Res.*, **96**, 2675–2692.
- , 1998: On the origin and influence of Adélie Land bottom water. *Ocean, Ice and Atmosphere: Interactions at the Antarctic Continental Margin*, S. Jacobs, and R. Wiess, Eds., Vol. 75, Antarctic Research Series, Amer. Geophys. Union, 151–171.
- , and C. Wunsch, 1990: Mass, heat, salt and nutrient fluxes and budgets in the North Atlantic Ocean. *Deep-Sea Res.*, **38**, 355–377.
- Robbins, P. E., and J. M. Toole, 1997: The dissolved silica budget as a constraint on the meridional overturning circulation of the Indian Ocean. *Deep-Sea Res.*, **44**, 879–906.
- Roemmich, D., and T. McCallister, 1989: Large scale circulation of the North Pacific Ocean. *Progress in Oceanography*, Vol. 22, Pergamon, 171–204.
- Roether, W., R. Schlitzer, A. Putzka, P. Beining, K. Bulsiewicz, G. Rohardt, and F. Delahoyde, 1993: A chlorofluoromethane and hydrographic section across Drake Passage: Deep water ventilation and meridional property transport. *J. Geophys. Res.*, **98**, 14423–14435.
- Rosenberg, M., R. Eriksen, S. Bell, and S. Rintoul, 1997: Aurora Australis Marine Science Cruise AU9404—Oceanographic field measurements and analysis. Tech. Rep. 8, Cooperative Research Centre for Antarctic and Southern Ocean Environments (ANTARCTIC CRC), 53 pp. [Available from Antarctic CRC, GPO Box 252-80, Hobart, Tasmania 7001, Australia].
- Saunders, P. M., and B. R. King, 1995: Oceanic fluxes on the WOCE A11 section. *J. Phys. Oceanogr.*, **25**, 1942–1957.
- SAVE, 1992a: South Atlantic Ventilation Experiment (SAVE), chemistry, physical and CTD data: Legs 1, 2 and 3. Tech. Rep. 92-9, 729 pp. [Available from Scripps Institution of Oceanography, University of California, San Diego, La Jolla, CA 92093-0224].
- , 1992b: South Atlantic Ventilation Experiment (SAVE), chemistry, physical and CTD data: Legs 4 and 5. Tech. Rep. 92-10, 625 pp. [Available from Scripps Institution of Oceanography, University of California, San Diego, La Jolla, CA 92093-0224].
- Schlitzer, R., 1987: Renewal rates of east Atlantic deep water estimated by inversion of  $^{14}\text{C}$ . *J. Geophys. Res.*, **92**, 2953–2969.
- Schmitz, W. J., Jr., 1995: On the interbasin-scale thermohaline circulation. *Rev. Geophys.*, **33**, 151–173.
- , 1996: On the World Ocean circulation. Vol. II: The Pacific and Indian Oceans/A global update. Tech. Rep. WHOI-96-08, 237 pp. [Available from Woods Hole Oceanographic Institute, Woods Hole, MA 02543].
- Sloyan, B. M., 1997: The circulation of the Southern Ocean and the adjacent ocean basins determined by inverse methods. Ph.D. thesis,

- , and S. R. Rintoul, 2000: The Southern Ocean limb of the global deep overturning circulation. *J. Phys. Oceanogr.*, in press.
- Speer, K., and E. Tziperman, 1992: Rates of water mass formation in the North Atlantic Ocean. *J. Phys. Oceanogr.*, **22**, 93–104.
- , and W. Zenk, 1993: The flow of Antarctic Bottom Water into the Brazil Basin. *J. Phys. Oceanogr.*, **23**, 2667–2682.
- Stommel, H., and A. B. Arons, 1960: On the abyssal circulation of the world's ocean—ii: An idealized model of circulation pattern and amplitude in oceanic basins. *Deep-Sea Res.*, **6**, 140–154.
- Stramma, L., and R. G. Peterson, 1990: The South Atlantic Current. *J. Phys. Oceanogr.*, **20**, 846–859.
- Talley, L. D., 1996: Antarctic Intermediate Water in the South Atlantic. *The South Atlantic: Present and Past Circulation*, G. Wefer, W. H. Berger, G. Siedler, and D. J. Webb, Eds., Springer-Verlag, 219–238.
- Toggweiler, J. R., and B. Samuels, 1993: New radiocarbon constraints on the upwelling of abyssal water to the ocean's surface. *The Global Carbon Cycle*. NATO ASI Series I: Global Environmental Change, Vol. 15, M. Heimann, Ed., Springer-Verlag, 333–363.
- , and —, 1998: On the ocean's large-scale circulation near limit of no vertical mixing. *J. Phys. Oceanogr.*, **28**, 1832–1852.
- Toole, J. M., and B. A. Warren, 1993: A hydrographic section across the Subtropical South Indian Ocean. *Deep-Sea Res.*, **40**, 1973–2019.
- Truesdale, P., D. M. Nelson, A. J. Van Bennekom, D. J. DeMaster, A. Leynaert, and B. Quinlan, 1995: The silica balance in the world ocean: A reestimate. *Science*, **268**, 375–379.
- Tsimplis, M. N., S. Bacon, and H. L. Bryden, 1998: The circulation of the subtropical South Pacific derived from hydrographic data. *J. Geophys. Res.*, **103**, 21443–21468.
- Tziperman, E., and A. Hecht, 1988: Circulation in the eastern Levantine Basin determined by inverse methods. *J. Phys. Oceanogr.*, **18**, 506–518.
- Walín, G., 1982: On the relation between sea-surface heat flow and thermal circulation in the ocean. *Tellus*, **34**, 187–195.
- Warren, B., 1981a: Transindian hydrographic section at lat. 18°S: Property distribution and circulation in the South Indian Ocean. *Deep-Sea Res.*, **28**, 759–788.
- , 1981b: Deep circulation of the World Ocean. *Evolution of Physical Oceanography*, B. A. Warren and C. Wunsch, Eds., The MIT Press, 6–41.
- , and K. G. Speer, 1991: Deep circulation in the eastern South Atlantic Ocean. *Deep-Sea Res.*, **38**, S281–S322.
- Whitworth, T., III, and W. D. Nowlin Jr., 1987: Water masses and currents of the Southern Ocean at the Greenwich Meridian. *J. Geophys. Res.*, **92**, 6462–6476.
- , —, R. D. Pillsbury, and R. F. Weiss, 1991: Observations of the Antarctic Circumpolar Current and deep boundary current in the Southwest Atlantic. *J. Geophys. Res.*, **96**, 15105–15118.
- , B. A. Warren, W. D. Nowlin Jr., R. D. Pillsbury, and M. I. Moore, 1999: On the deep western-boundary current in the southwest Pacific Basin. *Progress in Oceanography*, Vol. 43, Pergamon, 1–54.
- Wong, A. P. S., N. L. Bindoff, and A. Forbes, 1998: Ocean–ice shelf interactions and possible bottom water formation in Prydz Bay, Antarctica. *Ocean, Ice and Atmosphere: Interactions at the Antarctic Continental Margin*. S. Jacobs and R. Wiess, Eds., Vol. 75, Antarctic Research Series, Amer. Geophys. Union, 173–187.
- Wunsch, C., 1970: On oceanic boundary mixing. *Deep-Sea Res.*, **17**, 293–301.
- , 1978: The North Atlantic general circulation west of 50°W determined by inverse methods. *Rev. Geophys. Space Phys.*, **16** (4), 583–620.
- , 1984: An eclectic Atlantic Ocean circulation model. I: The meridional flux of heat. *J. Phys. Oceanogr.*, **14**, 1712–1732.
- , 1996: *The Ocean Circulation Inverse Problem*. Cambridge University Press, 441 pp.
- , D. Hu, and B. Grant, 1983: Mass, heat, salt and nutrient fluxes in the South Pacific Ocean. *J. Phys. Oceanogr.*, **13**, 725–753.

## APPENDIX

### 7. Parameterization of Diapycnal Fluxes

In order to assess the accuracy of the parameterization of diapycnal fluxes in the inverse box model, and for guidance in their interpretation, we use output from a numerical model. This is an extension of an earlier study by [McIntosh and Rintoul \(1997\)](#). For details of both FRAM and the FRAM-derived inverse model the reader is referred to [McIntosh and Rintoul \(1997\)](#).

Experiments are performed using two forms of the conservation equations. First, following [McIntosh and Rintoul \(1997\)](#), a system of simultaneous equations is solved for the unknown reference level velocities ( $b$ ) and the unknown net diapycnal fluxes for mass, heat, and salt ( $w_c^* = w_m^*, w_t^*, w_s^*$ ):

$$\sum_{j=1}^N \Delta x_j \int_{h_m}^{h_{m+1}} \rho C_j (v_r + b)_j dp + E_j C_j + (w_c^* AC)_m - (w_c^* AC)_{m+1} = 0, \quad (\text{A1})$$

where  $\Delta x_j$  is the station spacing at pair  $j$ .

The second formulation of the inverse problem also solves for the reference level velocities ( $b_j$ ) and the diapycnal fluxes, but the latter are represented as a mean advective flux plus a (Fickian) diffusive flux:

$$\sum_{j=1}^N \Delta x_j \int_{h_m}^{h_{m+1}} \rho C_j (v_r + b)_j dp + E_j C_j + (eAC)_m - (eAC)_{m+1} + \left( \kappa_c^* A \frac{dC}{dz} \right)_m - \left( \kappa_c^* A \frac{dC}{dz} \right)_{m+1} \approx 0. \quad (\text{A2})$$

In [Eq. \(A2\)](#)  $(eAC)_m$  is the diapycnal flux of property  $C$  due to advection and

$$\left( \kappa_c^* A \frac{dC}{dz} \right)_m$$

represents the effective diapycnal diffusive flux of  $C$ . The property gradients  $dC/dz$  are diagnosed directly from FRAM, and averaged over the interface area. The unknowns to be determined are  $b_j$  reference velocity;  $e_m$  the diapycnal advective velocity across each interface (the same for all properties), and  $\kappa_c^*$  the effective diffusivity for heat and salt across each interface. The diffusivity found is the “effective” diffusivity in the sense that it represents the contribution to the net diapycnal flux of all processes other than advection by the mean diapycnal velocity. The two parameterizations of the diapycnal fluxes are compared to the “true” FRAM solution.

The reference velocities of the two inverse solutions are very similar and are a smoothed representation of the FRAM velocities. Although the inverse reference velocities are very smooth, they still contain enough information to reproduce the associated mass fluxes. [Table A1](#) gives the comparison of the “true” FRAM mass, heat, and salt anomaly fluxes at 117°E and 147°E with the two inverse models.

A comparison of the total diapycnal property fluxes between the inverse solutions and FRAM for the polar frontal zone south of Australia is shown in [Fig. A1](#). Both inverse solutions give similar estimates of the net diapycnal property flux, which accurately reproduce the “true” FRAM diapycnal property flux. For the polar frontal zone the rms differences between the “true” FRAM diapycnal flux and the two inverse solutions are  $0.51 \times 10^6 \text{ m}^3 \text{ s}^{-1}$  and  $0.58 \times 10^6 \text{ m}^3 \text{ s}^{-1}$  for



diapycnal mass flux,  $2.8 \times 10^6 \text{ }^\circ\text{C m}^3 \text{ s}^{-1}$  and  $3.2 \times 10^6 \text{ }^\circ\text{C m}^3 \text{ s}^{-1}$  for diapycnal heat flux and  $169 \text{ (psu-35) m}^3 \text{ s}^{-1}$  and  $182 \text{ (psu-35) m}^3 \text{ s}^{-1}$  for diapycnal salt flux. The reader is reminded that in Fig. A1 salt diapycnal flux is expressed in units of  $\times 10^6 \text{ (psu-35) m}^3 \text{ s}^{-1}$ . Similar agreement is found in the other regions south of Australia (Sloyan 1997).

The “true” FRAM diapycnal “diffusivity” was diagnosed in two steps. First the “eddy” flux ( $\overline{e'c'}$ ) was calculated by subtracting the mean advective flux from the total advective flux. In this study the eddy flux ( $\overline{e'c'}$ ) is the flux due to correlations between spatial variations of the diapycnal velocity and tracer concentration about their mean value on each neutral surface. The eddy fluxes ( $\overline{e'c'}$ ) were then added to the diapycnal diffusive fluxes diagnosed from the model to give the “effective diffusive” flux in FRAM. Note that the diapycnal diffusion in FRAM includes a contribution from both horizontal and vertical diffusivity acting on the sloping isopycnals. These “effective diffusive” fluxes were then divided by the diapycnal property gradient averaged along the neutral surface to give the “true” FRAM “effective diapycnal diffusivity.” The “effective diffusivity” diagnosed from FRAM in this way is the equivalent of the diffusivity; which we can calculate from the inverse model: a surface average of all processes other than mean advection that transport properties across neutral surfaces.

A comparison between the “effective diffusivities” of heat and salt in FRAM and the inverse solutions for the subantarctic and polar frontal zones south of Australia are shown in Fig. A2. Also plotted in Fig. A2 is the explicit FRAM vertical heat and salt diffusivity ( $5 \times 10^{-5} \text{ m}^2 \text{ s}^{-1}$ ). The “true” FRAM heat and salt diapycnal diffusivities are different from the prescribed vertical diffusivity in FRAM, particularly across the lightest and densest layers which correspond to outcropping or undercropping layers, respectively. In part this is due to the fact that the diapycnal diffusivity includes contributions from horizontal mixing across sloping isopycnals, as described above. A more important factor is that the diagnosed “effective diapycnal diffusivity” includes all processes carrying properties across isopycnals. Of particular importance in FRAM is the flux due to correlations between variations of diapycnal velocity and variations of tracer concentration on an isopycnal surface ( $\overline{e'c'}$ ).

Figure A3 shows the size of  $\overline{e'c'}$  on particular layers within the polar frontal zone. Layers 7 and 8 have large  $\overline{e'c'}$  on their outcropping edges and in some internal grid boxes, while on layer 17, which does not outcrop,  $\overline{e'c'}$  is very small. The inclusion of the eddy terms in the diffusivity results in the large diffusivities in the outcropping layer of the subantarctic and polar frontal zones (Fig. A2). In contrast, the heat and salt diffusivities across the internal layers of the subantarctic zone are small, and agree with the explicit FRAM diffusivity. In the polar frontal zone there are numerous layers across which there are large diffusivities (the heat diffusivity is dominated by a particularly large diffusivity at layer 5). The strong frontal regions of the ACC and numerous outcropping layers result in a large  $\overline{e'c'}$  contribution to the net “effective diffusion.” Implications of the FRAM experiments for inversions of real data are discussed in section 3.

## Tables

Table 1. Hydrographic sections (year and austral season) used in this study and abbreviated name (Abbr) used in the text

Sections	Year (Season)	Abbr	Reference
SAVE2 11°S	1988 (summer)	SAVE2	SAVE (1992a)
SAVE2 10°-15°S	1989 (summer)	SAVE2	SAVE (1992b)
Drake Passage	1990 (summer)	DrakeP	Roether et al. (1992)
IAJAN-47°E	1984 (summer)	SAfrica	Whitworth and Nowlin (1987)
IAJAN-Weddell Sea	1984 (summer)	Wedsea	Whitworth and Nowlin (1987)
Indian 15°S	1976 (winter)	Ind15	Whalen (1984)
Indian 32°S	1987 (summer)	Ind32	Toole and Whalen (1993)
WOCE-282 140°E	1994 (summer)	Silica	Roeschberg et al. (1997)
WOCE-49 32°S	1992 (winter)	Pa32	Tomlinson et al. (1998)

Click on thumbnail for full-sized image.

Table 2. A priori constraints (+ve – north/eastward) applied to the inverse model. The inverse model conserves mass, heat, and salt in all layers while the silica conservation is conserved as a total section flux

Constraint	Transport
$-0.8 \times 10^6 \text{ m}^3 \text{ s}^{-1}$	Net southward transport at SAVE2 (Cookman and Nancarrow 1986)
$4 \times 10^6 \text{ m}^3 \text{ s}^{-1}$	Northward bottom transport to the Brazil Basin (Bjerg et al. 1982; Speer and Zook 1991)
$0 \times 10^6 \text{ m}^3 \text{ s}^{-1}$	Net transport across Wedsea
$10 \times 10^6 \text{ m}^3 \text{ s}^{-1}$	Heat loss over Weddell Sea (Gordon and Haber 1990; Fahrbach et al. 1994)
$80 \times 10^6 \text{ m}^3 \text{ s}^{-1}$	Northward Malabar Current (Peterson and Stramma 1991; Peterson 1992)
$6 \times 10^6 \text{ m}^3 \text{ s}^{-1}$	Northward transport A&SW across Argentine Basin (Whitworth et al. 1991)
$11 \times 10^6 \text{ m}^3 \text{ s}^{-1}$	Northward transport across WOCE PCM32 (Whitworth et al. 1999)
Silica	Conservation all regions (Trüger et al. 1995)

Click on thumbnail for full-sized image.

Table 3. Total section property fluxes (+ve – northward/eastward). Heat fluxes are relative to  $0^\circ\text{C}$  and converted to PW (1 PW =  $244 \times 10^6 \text{ }^\circ\text{C m}^3 \text{ s}^{-1}$ ). Units: mass  $\times 10^6 \text{ m}^3 \text{ s}^{-1}$ ; heat: PW  $\times 10^{15} \text{ W}$ ; salt  $\times 10^6 \text{ kg s}^{-1}$ ; freshwater  $\times 10^9 \text{ kg s}^{-1}$ ; silica  $\text{kmol s}^{-1}$

Property	Flux
Mass	
Heat	
Salt	
Freshwater	
Silica	

Click on thumbnail for full-sized image.

Table 4. Summary of mass fluxes ( $\times 10^6 \text{ m}^3 \text{ s}^{-1}$ , +ve – north/eastward). The individual layers have been grouped into five water classes as TW: surface and thermocline water; IW:intermediate water; UDW: upper deep water; LDW: lower deep water; and BW: bottom water. Also given are the neutral density ( $\gamma^n$ ) interval and model layers each of the water classes span

Name	$\gamma^n$	Sections (Order in Table 1)									
		SW1	SW4	SW6P	SW6S	SW6E	SW11	SW12	SW13	SW14	SW15
FW	26.0-27.4	11.3	8.1	10.85	28.1	7	2.1	-8.2	40.1	-2.1	-8.3
IW	27.4-28.0	-9.1	-5.1	49.1	71.2	-1.03	-4.1	-20.1	80.1	-12.2	-12.2
UDW	28.0-28.5	-4.2	-10.2	20.1	40.1	-4.03	3.1	10.1	30.1	40.1	40.1
LDW	28.5-29.0	3.1	7.1	4.03	-2.03	4.1	1.02	10.2	4.1	4.1	4.03
BW	29.0-30.0										

Click on thumbnail for full-sized image.

Table A1. Comparison of the “true” FRAM mass ( $\times 10^6 \text{ m}^3 \text{ s}^{-1}$ ), heat ( $\times 10^6 \text{ }^\circ\text{C m}^3 \text{ s}^{-1}$ ), and salt anomaly [ $\times 10^6 (\text{psu}-35) \text{ m}^3 \text{ s}^{-1}$ ] with the inverse models. The initial guess (Initial\_g) mass, heat, and salt anomaly fluxes from the FRAM velocity shear relative to the bottom are also shown. Inv\_total is the inverse model that solves the total diapycnal property flux while Inv\_exp explicitly solves the diapycnal advection and diffusion property fluxes

Section	Property	“True”	Initial_g	Inv_total	Inv_exp
117E	Mass	194.9	211.3	191.0 $\pm$ 6.1	187.6 $\pm$ 6.1
	Heat	535.46	598.2	540.05 $\pm$ 15.55	528.09 $\pm$ 15.54
	Salt An.	-90.39	-90.53	-89.21 $\pm$ 1.18	-89.13 $\pm$ 1.00
117E	Mass	194.9	170.5	191.0 $\pm$ 3.3	187.6 $\pm$ 3.3
	Heat	548.29	527.57	553.99 $\pm$ 7.02	553.13 $\pm$ 7.02
	Salt An.	-92.52	-83.55	-91.08 $\pm$ 1.01	-89.99 $\pm$ 1.00

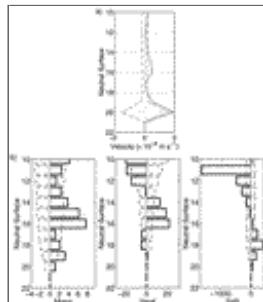
Click on thumbnail for full-sized image.

## Figures



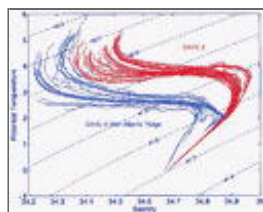
Click on thumbnail for full-sized image.

Fig. 1. Location of hydrographic sections and box regions used in the inverse model



Click on thumbnail for full-sized image.

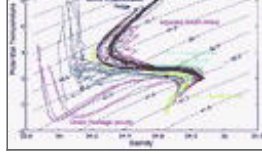
Fig. 2. A comparison of (a) the diapycnal mass velocity ( $\text{m s}^{-1}$ ) and (b) the associated diapycnal property fluxes for the subtropical Atlantic (Box I): mass  $\times 10^6 \text{ m}^3 \text{ s}^{-1}$ , heat  $\times 10^6 \text{ }^\circ\text{C m}^3 \text{ s}^{-1}$ , and salt  $\times 10^6 \text{ kg s}^{-1}$ . Positive “velocities” and fluxes are upward (i.e., toward less dense water masses). The diapycnal mass velocity standard deviation and property diapycnal flux error (dot-dashed) is also shown



Click on thumbnail for full-sized image.

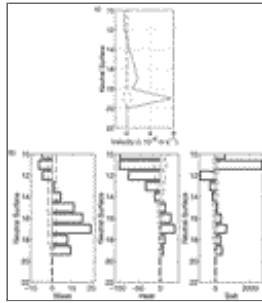
Fig. 3. Potential temperature ( $^\circ\text{C}$ ) and salinity ( $S$ ) for SAVE2 and the hydrographic stations over the Mid-Atlantic Ridge at SAVE4. Contour lines are potential density reference to 3000 dbar. Note that the temperature and salinity properties of NADW (41.1–41.5) are significantly modified in the subtropical Atlantic by mixing with AABW (41.5–41.7), CDW (41.1–41.5), and overlying intermediate water (40.5–41.1) in the Brazil and Argentine Basins





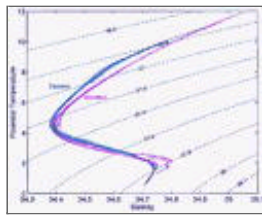
[Click on thumbnail for full-sized image.](#)

Fig. 4. Potential temperature ( $^{\circ}\text{C}$ ) and salinity ( $S$ ) of intermediate SAMW/AAIW 30.9–32.1, CDW/NADW 41.1–41.5, and AABW 41.5–41.7. Contour lines are potential density referenced to 1000 dbar for  $\theta > 3^{\circ}\text{C}$  and referenced to 3000 dbar for  $\theta < 3^{\circ}\text{C}$



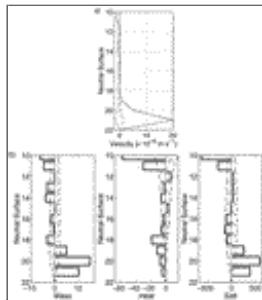
[Click on thumbnail for full-sized image.](#)

Fig. 5. A comparison of (a) the diapycnal mass velocity ( $\text{m s}^{-1}$ ) and (b) the associated diapycnal property fluxes for the subtropical Indian (Box IV): mass  $\times 10^6 \text{ m}^3 \text{ s}^{-1}$ , heat  $\times 10^6 \text{ }^{\circ}\text{C m}^3 \text{ s}^{-1}$ , and salt  $\times 10^6 \text{ kg s}^{-1}$ . Positive “velocities” and fluxes are upward (i.e., toward less dense water masses). The diapycnal mass velocity standard deviation and property diapycnal flux error (dot-dashed) is also shown



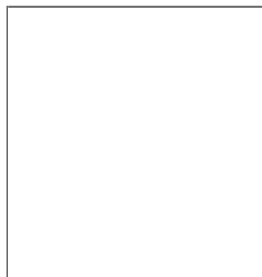
[Click on thumbnail for full-sized image.](#)

Fig. 6. Potential temperature ( $^{\circ}\text{C}$ ) and salinity ( $S$ ) of intermediate water (SAMW/AAIW 26.8– 27.4) across Ind32 in the eastern (Crozet, Central Indian, and Perth Basins) and western (Natal, Mozambique, and Madagascar Basins). Contour lines are potential density referenced to 0 dbar



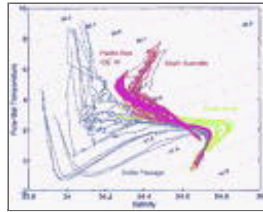
[Click on thumbnail for full-sized image.](#)

Fig. 7. A comparison of (a) the diapycnal mass velocity ( $\text{m s}^{-1}$ ) and (b) the associated diapycnal property fluxes for the Southern Ocean Atlantic sector (Box II) — mass  $\times 10^6 \text{ m}^3 \text{ s}^{-1}$ , heat  $\times 10^6 \text{ }^{\circ}\text{C m}^3 \text{ s}^{-1}$ , and salt  $\times 10^6 \text{ kg s}^{-1}$ . Positive “velocities” and fluxes are upward (i.e., toward less dense water masses). The diapycnal mass velocity standard deviation and property diapycnal flux error (dot-dashed) is also shown



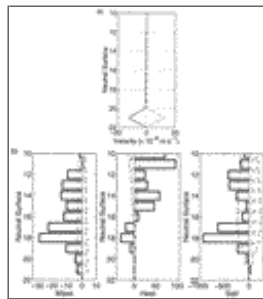
[Click on thumbnail for full-sized image.](#)

Fig. 8. A comparison of (a) the diapycnal mass velocity ( $\text{m s}^{-1}$ ) and (b) the associated diapycnal property fluxes for the Southern Ocean Indian sector (Box V) — mass  $\times 10^6 \text{ m}^3 \text{ s}^{-1}$ , heat  $\times 10^6 \text{ }^\circ\text{C m}^3 \text{ s}^{-1}$ , and salt  $\times 10^6 \text{ kg s}^{-1}$ . Positive “velocities” and fluxes are upward (i.e., toward less dense water masses). The diapycnal mass velocity standard deviation and property diapycnal flux error (dot-dashed) is also shown



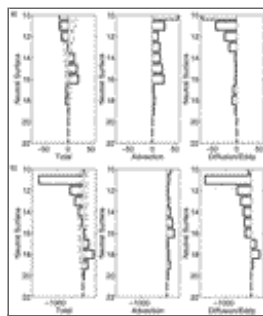
[Click on thumbnail for full-sized image.](#)

Fig. 9. Potential temperature ( $^\circ\text{C}$ ) and salinity ( $S$ ) south of Africa, south of Australia,  $32^\circ\text{S}$  Pacific Ocean east of  $130^\circ\text{W}$ , and at Drake Passage. CDW/NADW defined between  $41.1\text{--}41.5$ , AABW  $41.5\text{--}41.9$  and SAMW/AAIW  $39.7\text{--}41.1$ . Contour lines are potential density referenced to  $3000 \text{ db}$



[Click on thumbnail for full-sized image.](#)

Fig. 10. A comparison of (a) the diapycnal mass velocity ( $\text{m s}^{-1}$ ) and (b) the associated diapycnal property fluxes for the the Southern Ocean Pacific sector (Box IV): mass  $\times 10^6 \text{ m}^3 \text{ s}^{-1}$ , heat  $\times 10^6 \text{ }^\circ\text{C m}^3 \text{ s}^{-1}$ , and salt  $\times 10^6 \text{ kg s}^{-1}$ . Positive “velocities” and fluxes are upward (i.e., toward less dense water masses). The diapycnal mass velocity standard deviation and property diapycnal flux error (dot-dashed) is also shown



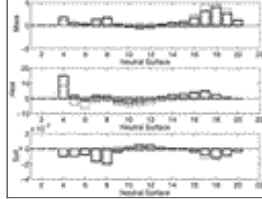
[Click on thumbnail for full-sized image.](#)

Fig. 11. A breakdown of (a) the net diapycnal heat flux ( $w_h^* \times \bar{\theta}$ ) into the mean advection ( $w_m^* \times \bar{\theta}$ ) and effective diffusion (diffusion plus eddy flux), as a residual ( $w_h^* \times \bar{\theta} - w_m^* \times \bar{\theta}$ ). Units  $\times 10^6 \text{ }^\circ\text{C m}^3 \text{ s}^{-1}$ . (b) The net diapycnal salt flux ( $w_s^* \times \bar{S}$ ), salt flux carried by mean advection ( $w_m^* \times \bar{S}$ ) and effective diffusion (diffusion plus eddy flux), as a residual ( $w_s^* \times \bar{S} - w_m^* \times \bar{S}$ ) flux. Units  $\times 10^6 \text{ kg s}^{-1}$ . For the subtropical Atlantic (Box I). The total property diapycnal flux error (dot-dashed) is also shown



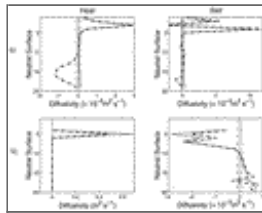
Click on thumbnail for full-sized image.

Fig. 12. A breakdown of (a) the net diapycnal heat flux ( $w_h^* \times \bar{\theta}$ ) into the mean advection ( $w_m^* \times \bar{\theta}$ ) and effective diffusion (diffusion plus eddy flux), as a residual ( $w_h^* \times \bar{\theta} - w_m^* \times \bar{\theta}$ ). Units  $\times 10^6 \text{ }^\circ\text{C m}^3 \text{ s}^{-1}$ . (b) The net diapycnal salt flux ( $w_s^* \times \bar{S}$ ), salt flux carried by mean advection ( $w_m^* \times \bar{S}$ ) and effective diffusion (diffusion plus eddy flux), as a residual ( $w_s^* \times \bar{S} - w_m^* \times \bar{S}$ ) flux. Units  $\times 10^6 \text{ kg s}^{-1}$ . For the Southern Ocean Indian sector (Box V). The total property diapycnal flux error (dot-dashed) is also shown



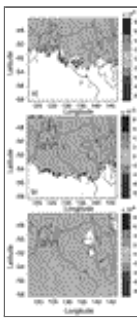
Click on thumbnail for full-sized image.

Fig. A1. The total diapycnal mass ( $\times 10^6 \text{ m}^3 \text{ s}^{-1}$ , upper), heat ( $\times 10^6 \text{ }^\circ\text{C m}^3 \text{ s}^{-1}$ , middle) and salt anomaly [ $\times 10^6 \text{ (psu-35) m}^3 \text{ s}^{-1}$ , lower] flux a region south of Australia between 117°E and 147°E and 46°S and 58°S. This box encloses the polar frontal zone, which includes the Subantarctic and Antarctic Polar fronts (Sloyan 1997). “True” FRAM diapycnal flux (thin solid), the inverse model (dashed) that solves the total property flux and inverse model (thick solid) the explicitly solves the diapycnal advection and property diffusion. Shaded bars are the errors associated with the inverse derived fluxes



Click on thumbnail for full-sized image.

Fig. A2. Comparison of diapycnal effective heat and salt diffusivity between “true” FRAM (solid), and inverse solution with explicit diapycnal advection and effective diffusion (dot-dashed) for (a) the subantarctic zone between 42°S and 46°S, 117° and 147°E and (b) the polar frontal zone defined in Fig. A1. The solution standard deviation (dot-dashed) is unchanged from the a priori values of  $1 \times 10^{-4} \text{ m}^2 \text{ s}^{-1}$ . The actual FRAM heat and salt diffusivity of  $5 \times 10^{-5} \text{ m}^2 \text{ s}^{-1}$  is also shown



Click on thumbnail for full-sized image.

Fig. A3. Evaluation of the heat flux ( $\times 10^6 \text{ }^\circ\text{C m}^3 \text{ s}^{-1}$ ) due to  $e'c'$  for the polar frontal zone defined in Fig. A1 on neutral surface layers (a) layer 7, (b) layer 8, and (c) layer 17. The 3000-m and 4000-m contour depth are also shown. These show that larger eddy term on interior grid boxes of layers 7 and 8 probably reflect topographic mixing



© 2008 American Meteorological Society [Privacy Policy and Disclaimer](#)  
Headquarters: 45 Beacon Street Boston, MA 02108-3693  
DC Office: 1120 G Street, NW, Suite 800 Washington DC, 20005-3826  
[amsinfo@ametsoc.org](mailto:amsinfo@ametsoc.org) Phone: 617-227-2425 Fax: 617-742-8718  
[Allen Press, Inc.](#) assists in the online publication of *AMS* journals.